Supporting Information

Rationally designed carbon-encapsulated manganese selenides composites from metal-organic frameworks for stable aqueous aqueous Zn-Mn batteries

*Bin Wang[1], Wenqi Li[1], Siyuan Wang[1], Peng Xie[1], Peng Wan[1], Ying Gui[1], Ding Chen[1]**

[1]State Key Laboratory of Advanced Design and Manufacturing for Vehicle Body, College of Mechanical and Vehicle Engineering, Hunan University, 410082 Changsha, China

*Corresponding author: chending@hnu.edu.cn (D. Chen)

S1. CALCULATION EQUATIONS

During the electrochemical kinetic analysis-based CV curves, the peak current (i) and scan rate (v) can be obeyed with Equations. 1-2[1, 2]:

$$i = av^b \quad (1)$$

$$\log(i) = b\log(v) + \log(a) \quad (2)$$

where a and b are the fitted parameters. The current $i(V)$ at a given potential V obey the relations of [3]

$$i(V) = k_1 v + k_2 v^{1/2} \quad (3)$$

and

$$i(V)/v^{1/2} = k_1/v^{1/2} + k_2 \quad (4)$$

Where $i(V)$, k_1v, and $k_2v^{1/2}$ correspond to the measured current, current from the surface capacitive contribution, and current from diffusion-controlled Zn^{2+} intercalation contribution, respectively.

The ions diffusion coefficient can be well calculated from the low-frequency plots using the following equation (5):

$$D = \frac{R^2T^2}{2A^2n^4F^4C^2\sigma^2} \quad (5)$$

where R is the gas constant, T is the absolute temperature, A is the surface area of electrode, n is the number of electrons per molecule during oxidization, F is the Faraday constant, C is the concentration of ion, and σ is the Warburg factor, where the Warburg factor is related to Z′ derived by the following equation (6)[4]:

$$Z' = R_s + R_{ct} + \sigma\omega^{-1/2} \quad (6)$$

Where ω is the angular frequency in the region, R_s is the ohmic resistance, R_{ct} is the charge-transfer resistance.

The ions diffusion coefficients were also measured by Galvanostatic Intermittent Titration Technique (GITT) and calculated based on the equation (7) below[5]:

$$D_{GITT} = \frac{4}{\pi\tau}\left(\frac{m_B V_m}{M_B S}\right)^2 \left(\frac{\Delta E_s}{\Delta E_\tau}\right)^2 \quad (7)$$

Where m_B (g) is the weight of the active materials, M_B (g mol^{-1}) is the molecular weight, V_m (cm^3 mol^{-1}) is its molar volume, S (cm^2) is the surface area, τ (s) is duration time of the current pulse, ΔE_s is the voltage difference measured at the end of the relaxation period for two successive steps, ΔE_τ is the difference between the initial voltage and final voltage during the discharge pulse time τ after eliminating the iR drop. It is also calculated D_{GITT} by equation (8) as follows[6]:

$$D_{GITT} = \frac{4L^2}{\pi\tau}\left(\frac{\Delta E_s}{\Delta E_\tau}\right)^2 \quad (8)$$

L is ion diffusion length (cm), for compact electrode, it is equal to the thickness of cathode material.

S2. Results

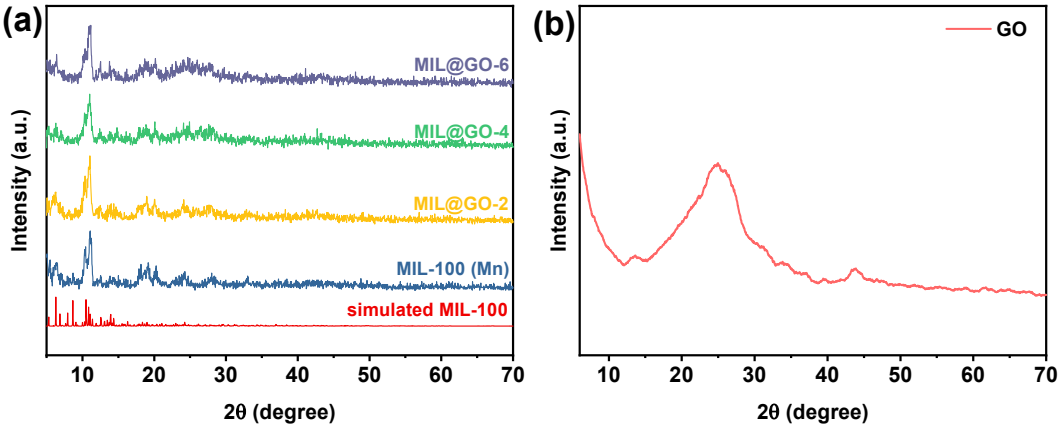

Figure S1. XRD spectrum for (a) MIL-100, MIL-GO-*x* and (b) GO.

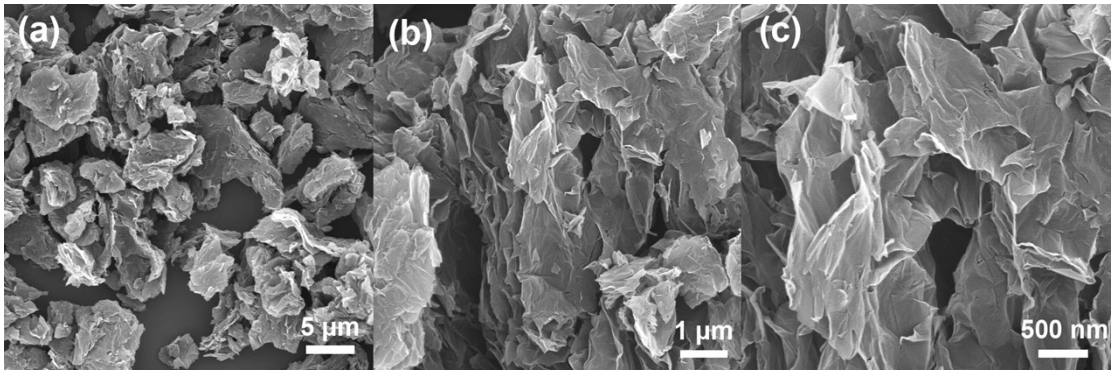

Figure S2. SEM images with different magnifications of GO, respectively. (a) 5 μm, (b) 1 μm, (c) 500 nm.

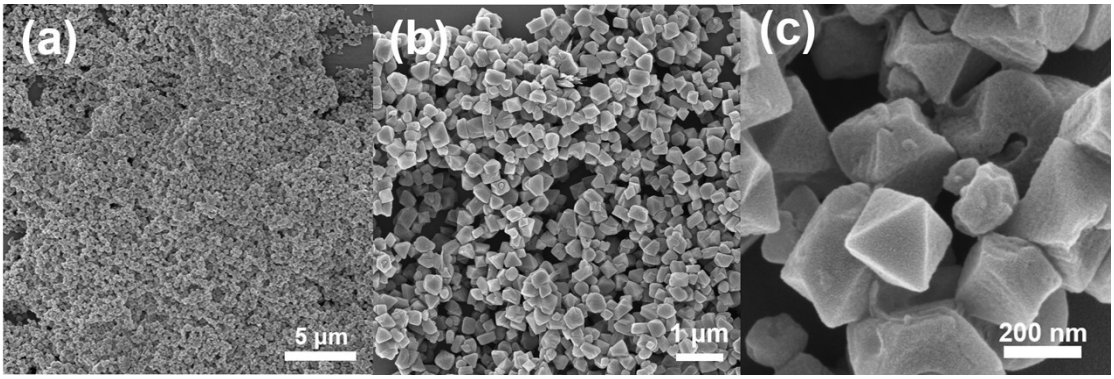

Figure S3. SEM images with different magnifications of MIL-100, respectively. (a) 5 μm, (b) 1 μm, (c) 200 nm.

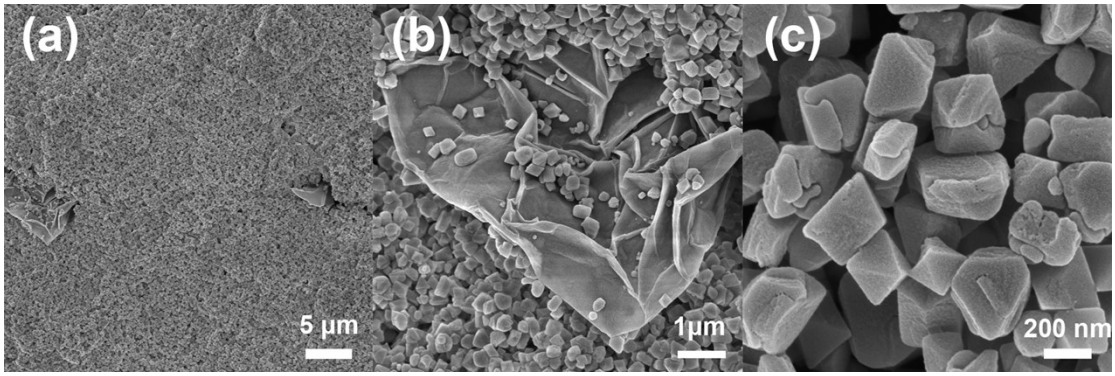

Figure S4. SEM images with different magnifications of MIL@GO-2, respectively. (a) 5 μm, (b) 1 μm, (c) 200 nm.

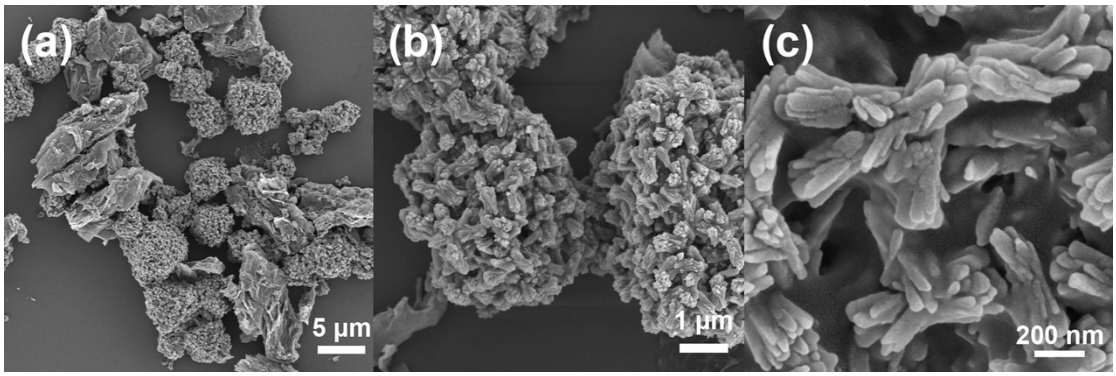

Figure S5. SEM images with different magnifications of MIL@GO-4, respectively. (a) 5 μm, (b) 1 μm, (c) 200 nm.

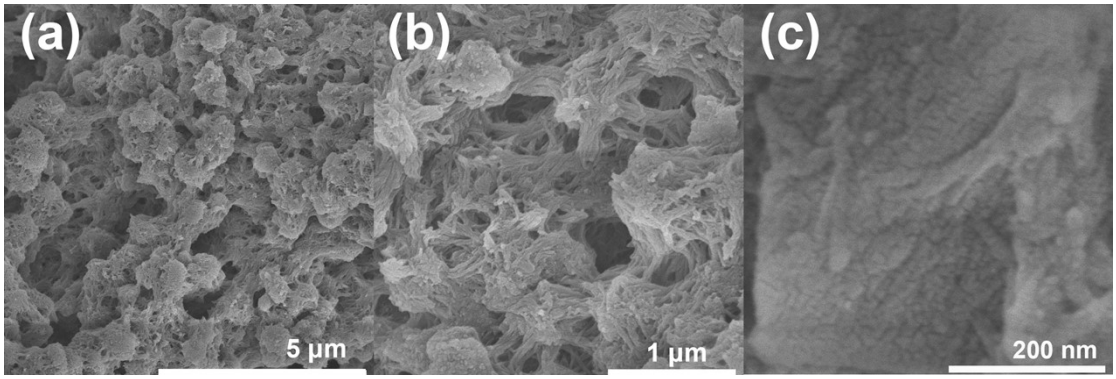

Figure S6. SEM images with different magnifications of MIL@GO-6, respectively. (a) 5 μm, (b) 1 μm, (c) 200 nm.

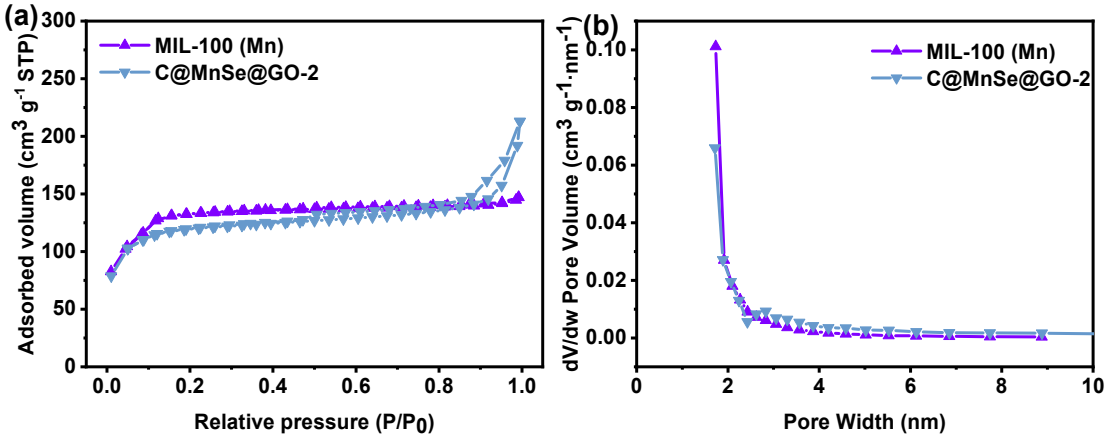

Figure S7. (a) N_2 adsorption-desorption isotherms and (b) pore size distributions of MIL-100 and C@MnSe@GO-2.

Figure S7 shows the N_2 adsorption and desorption curves of MIL-100 and C@MnSe@GO-2 and the corresponding pore size distributions. It can be seen in Figure S7a that all curves exhibit H3-type with hysteresis loops. MIL-100 exhibits a large specific surface area of about 500.86 m^2 g^{-1}, whereas the specific surface area of C@MnSe@GO-2 decreases slightly from 500.86 m^2 g^{-1} to 453.12 m^2 g^{-1} after the introduction of GO. However, owing to the high-temperature gas-phase selenization process, a carbon coating is formed on the surface of C@MnSe@GO-2. This carbon coating serves to increase the material's pore volume and pore size, providing additional reactive sites for zinc ions. As a result, the enhanced porosity contributes to the improved reactivity and facilitates a higher capacity for zinc ion reactions.

Table S1. The porous structure for MIL-100 and C@MnSe@GO-2.

Samples	S_{BET} (m^2 g^{-1})	V_{total} (cm^3 g^{-1})	Average pore size (nm)
MIL-100	500.86	0.23	1.82
MnSe@GO-2	453.12	0.33	2.90

S_{BET}: BET surface area, V_{total}: total pore volume calculated by density functional theory (DFT) method.

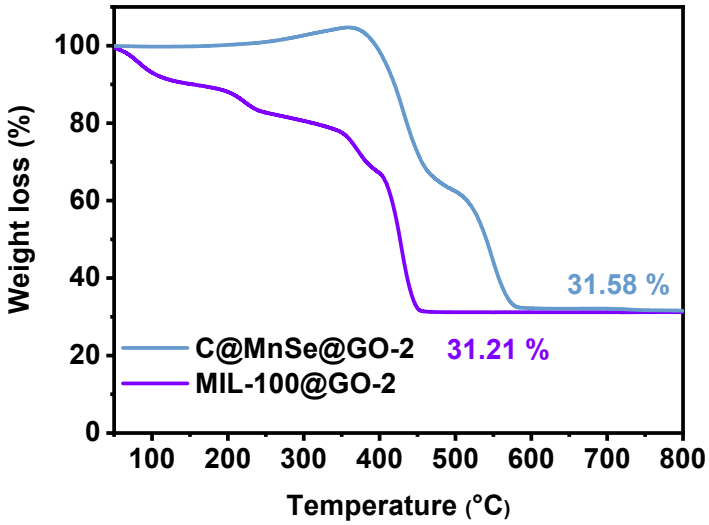

Figure S8. TGA curve of the C@MnSe@GO-2 and MIL-100@GO-2.

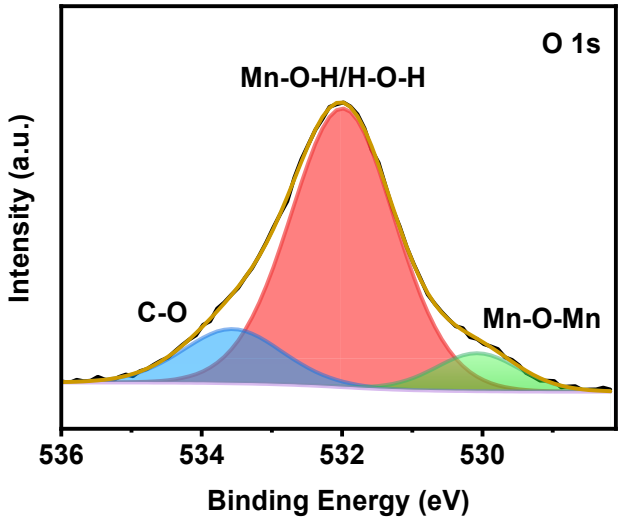

Figure S9. the O 1s high-resolution spectra of C@MnSe@GO-2

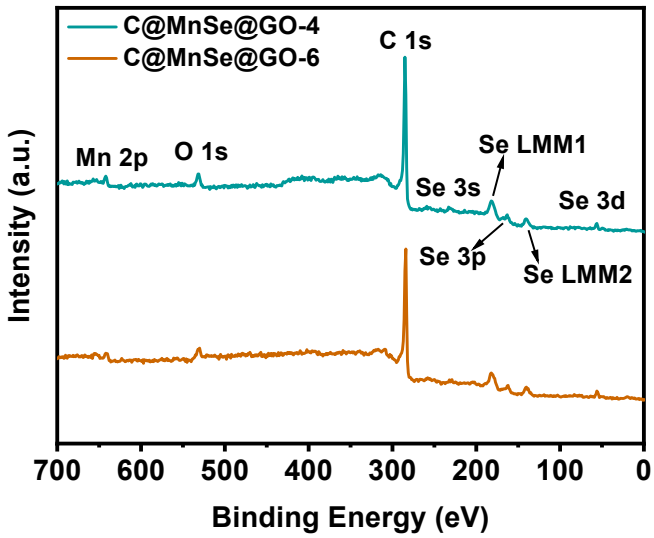

Figure S10. survey XPS spectrum of C@MnSe@GO-4 and C@MnSe@GO-6.

Table S2. The chemical compositions and contents of the C@MnSe@GO-*x* from XPS analysis.

Samples	C (at%)	Se (at%)	O (at%)	Mn (at%)
Binding energy (eV)	~284	~54	~532	~641/653
C@MnSe@GO-2	61.87	6.29	26.97	4.87
C@MnSe@GO-4	90.16	6.49	2.14	1.21
C@MnSe@GO-6	90.37	6.33	2.11	1.19

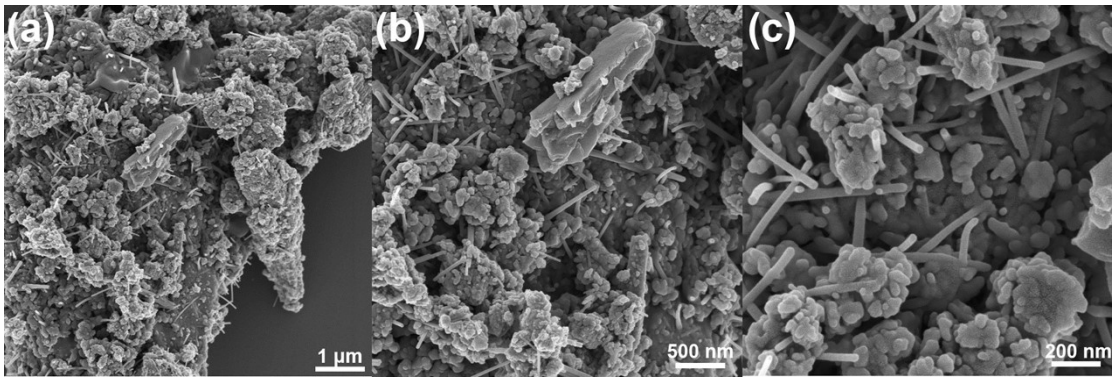

Figure S11. SEM images with different magnifications of Bulk MnO_2, respectively. (a) 1 μm, (b) 500 nm, (c) 200 nm.

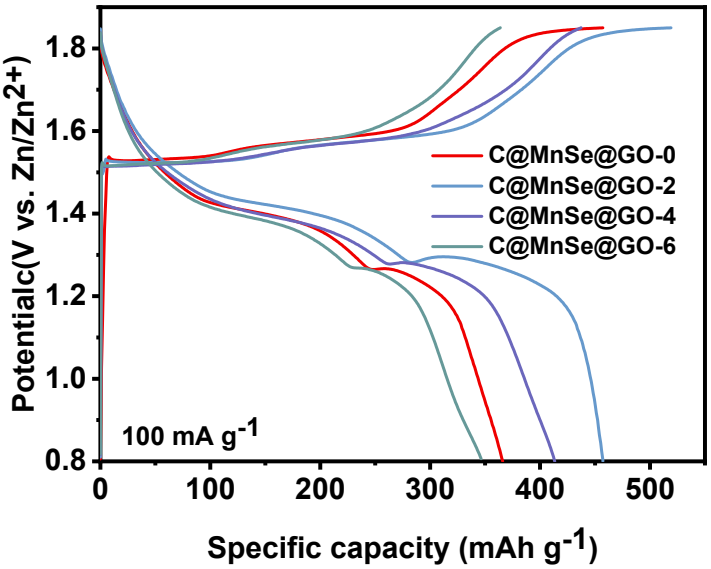

Figure S12. The galvanostatic charge-discharge curves for C@MnSe@GO-*x*.

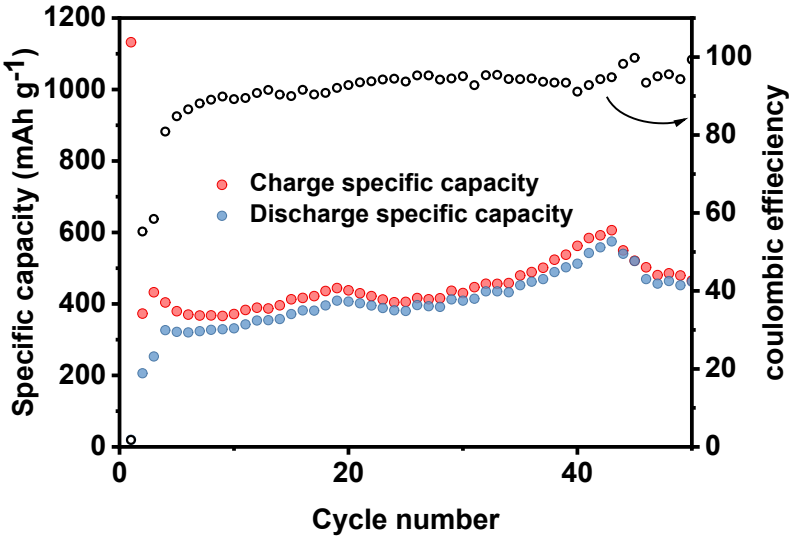

Figure S13. Cycling performance at 100 mA g-1 for C@MnSe@GO-2.

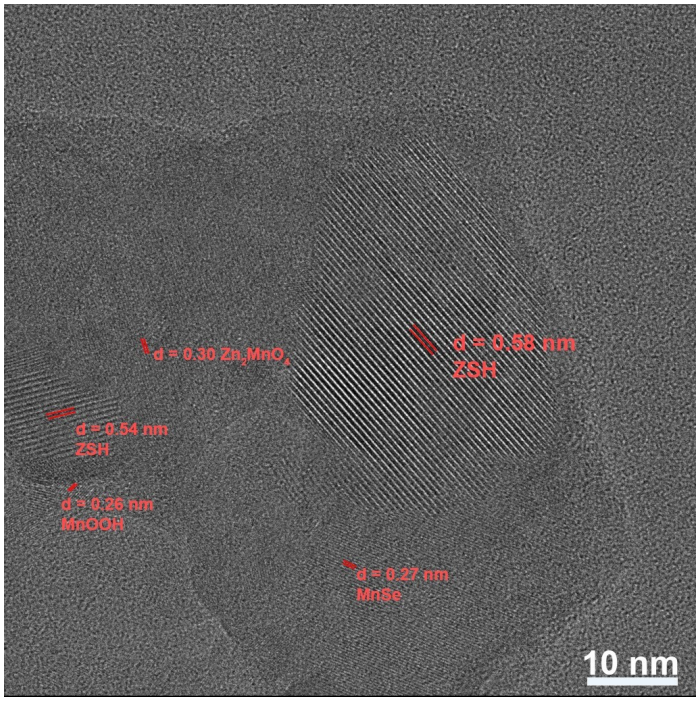

Figure S14. HRTEM images after Cycle test at 100 mA g^{-1} for C@MnSe@GO-2.

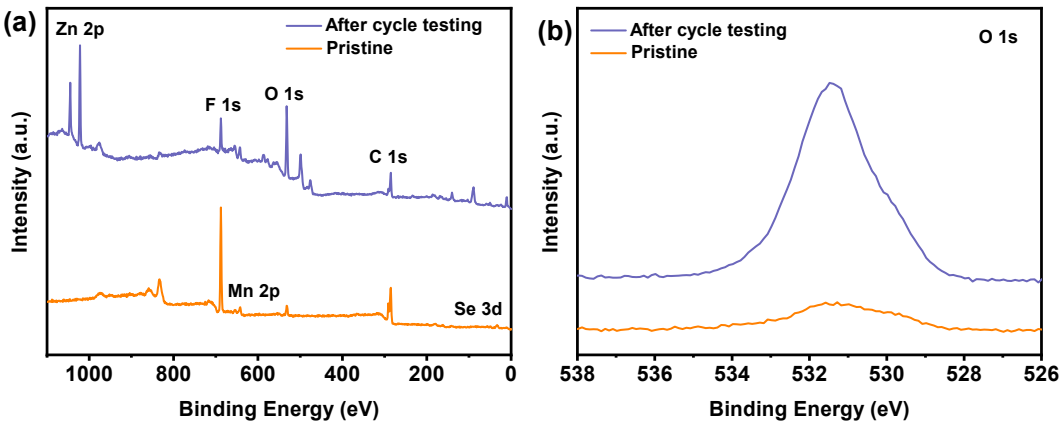

Figure S15. XPS images after Cycle test at 100 mA g^{-1} for C@MnSe@GO-2, (a) XPS survey, (b) O 1s.

Table S3 R_s and R_{ct} values fitted from the corresponding EIS plots.

Samples	R_s (ohm)	R_{ct} (ohm)
Bulk MnO_2	3.14	623.24
C@MnSe@GO-0	2.97	52.5
C@MnSe@GO-2	2.58	32.2

Table S4 *b* values fitted from the corresponding log(*i*) versus log(*v*) plots.

Samples	Anodic peak	Cathodic peak 1	Cathodic peak 2
C@MnSe@GO-0	$y = 0.84x - 0.14$	$y = 0.91x - 0.65$	$y = 0.88x - 0.48$
C@MnSe@GO-2	$y = 0.94x + 0.11$	$y = 0.72x - 0.54$	$y = 0.91x - 0.20$

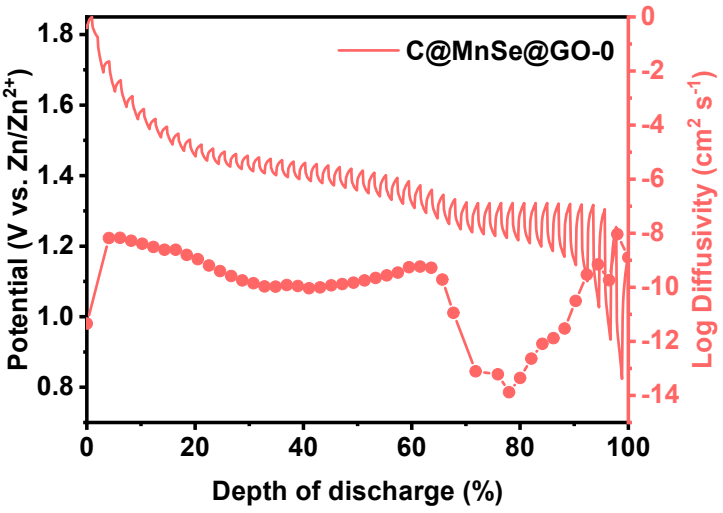

Figure S16. GITT and ionic diffusion coefficient curves during discharging for C@MnSe@GO-0.

Table S5 Comparison of the Zn ion storage performance of C@MnSe@GO-2 and other recently reported similar Zn-ion battery cathodes.

Materials	Voltage window (V)	Electrolyte	Current density	Specific capacity (mAh g^{-1})	Current density	Specific capacity (mAh g^{-1})	Ref
Se-in-$Cu[Co(CN)_6]$	0.1-2.1	4 m $Zn(OTf)_2$	200 mA g^{-1}	664.7	10000 mA g^{-1}	430.6	7
MnS-EDO	0.8-2.0	2M $ZnSO_4$/0.1 M $MnSO_4$	300 mA g^{-1}	335.7	3000 mA g^{-1}	104	8
MnS0.5Se0.5	0.8-1.85	2M $ZnSO_4$/0.2 M $MnSO_4$	100 mA g^{-1}	272.8	2000 mA g^{-1}	91.8	9
VS_2	0.4-1.0	1M $ZnSO_4$	100 mA g^{-1}	187	2000 mA g^{-1}	133	10
MnS	0.8-2.0	2M $ZnSO_4$/0.1 M $MnSO_4$	90 mA g^{-1}	297.7	3000 mA g^{-1}	36.6	11
MnSe@rGO	0.8-1.85	2M $ZnSO_4$/0.1 M $MnSO_4$	0.1 C	290	5 C	178	12
$MnSe_2$	0.8-1.85	2M $ZnSO_4$/0.1 M $MnSO_4$	100 mA g^{-1}	452.4	2000 mA g^{-1}	242.7	13
MnSe-EO	0.7-1.9	1M $ZnSO_4$/0.1 M $MnSO_4$	100 mA g^{-1}	309	10000 mA g^{-1}	125.9	14
MoSSe/rGO	0.3-1.3	2M $Zn(CF_3SO_3)_2$	200 mA g^{-1}	253.8	5000 mA g^{-1}	124.2	15
MnS/MnO@N–CF	0.8-1.9	2M ZnSO4/0.1 M $MnSO_4$	100 mA g^{-1}	257.8	2000 mA g^{-1}	128.7	16
Layered VSe_2	0-1.6	2M $ZnSO_4$	200 mA g^{-1}	250.6	5000 mA g^{-1}	132.6	17
rGO-VSe_2	0.2-1.4	2M $ZnSO_4$	500 mA g^{-1}	221.5	4000 mA g^{-1}	161	18
$MnSe_2$/CNTs	0.8-2.0	2M $ZnSO_4$/0.1 M $MnSO_4$	100 mA g^{-1}	451.1	3000 mA g^{-1}	126.3	19
VSe_{2-x}-SS	0.4-1.6	3M $Zn(CF_3SO_3)_2$	200 mA g^{-1}	241.2	4000 mA g^{-1}	230.1	20
VSe_2	0.4-1.6	2M $ZnSO_4$	100 mA g^{-1}	131.8	2000 mA g^{-1}	79.5	21
C@MnSe@GO-2	0.8-1.85	2M $ZnSO_4$/0.2 M $MnSO_4$	100 mA g^{-1}	459.81	2000 mA g^{-1}	283.67	This work

References

1. L. Xie, W. Xiao, X. Shi, J. Hong, J. Cai, K. Zhang, L. Shao and Z. Sun, *Chemical Communications*, 2022, **58**, 13807-13810.
2. Y. Zeng, Y. Wang, Q. Jin, Z. Pei, D. Luan, X. Zhang and X. W. D. Lou, *Angew Chem Int Ed Engl*, 2021, **60**, 25793-25798.
3. Y. Zhang, Z. Li, L. Gong, X. Wang, P. Hu and J. Liu, *Journal of Energy Chemistry*, 2023, **77**, 561-571.
4. P. Cai, K. Wang, J. Ning, X. He, M. Chen, Q. Li, H. Li, M. Zhou, W. Wang and K. Jiang, *Advanced Energy Materials*, 2022, **12**, 2202182.
5. W. Sun, F. Wang, S. Hou, C. Yang, X. Fan, Z. Ma, T. Gao, F. Han, R. Hu, M. Zhu and C. Wang, *J Am Chem Soc*, 2017, **139**, 9775-9778.
6. B. Wang, Y. Zeng, P. Chen, J. Hu, P. Gao, J. Xu, K. Guo and J. Liu, *ACS Applied Materials & Interfaces*, 2022, **14**, 36079-36091.
7. L. Ma, Y. Ying, S. Chen, Z. Chen, H. Li, H. Huang, L. Zhao and C. Zhi, *Advanced Energy Materials*, 2022, **12**, 2201322
8. X. Chen, W. L. a, Y. Xu, Z. Zeng, H. Tian, M. Velayutham, W. Shi, W. Li, C. Wang, D. Reed, V. V. Khramtsov, X. L. b and X. Liu, *Nano Energy*, 2020, **75**, 104869.
9. C. Guo, R. Zhou, X. Liu, R. Tang, W. Xi and Y. Zhu, *Small*, 2023, 2306237.
10. T. Jiao, Q. Yang, S. Wu, Z. Wang, D. Chen, D. Shen, B. Liu, J. Cheng, H. Li, L. Ma, C. Zhi and W. Zhang, *Journal of Materials Chemistry A*, 2019, **7**, 16330-16338.
11. S. Xu, S. Fan, W. Ma, J. Fan and G. Li, *Inorganic Chemistry Frontiers*, 2022, **9**, 1481-1489.
12. S. Wang, G. Zeng, Q. Sun, Y. Feng, X. Wang, X. Ma, J. Li, H. Zhang, J. Wen, J. Feng, L. Ci, A. Cabot and Y. Tian, *ACS Nano*, 2023, **17**, 13256-13268.
13. X. Li, J. Xie, G. Liu, J. Ding, B. Zhang, H. Zheng, L. Fan, Y. Tang and X. Ma, *Journal of Alloys and Compounds*, 2023, **937**, 168424.
14. A. Molaei Aghdam, S. Habibzadeh, M. Javanbakht, M. Ershadi and M. R. Ganjali, *ACS Applied Energy Materials*, 2023, **6**, 3225-3235.
15. H. Li, B. Chen, R. Gao, F. Xu, X. Wen, X. Zhong, C. Li, Z. Piao, N. Hu, X. Xiao, F. Shao, G. Zhou and J. Yang, *Nano Research*, 2023, **16**, 4933-4940.
16. F. Tang, X. Wu, Y. Shen, Y. Xiang, X. Wu, L. Xiong and X. Wu, *Energy Storage Materials*, 2022, **52**, 180-188.
17. L. Wang, Z. Wu, M. Jiang, J. Lu, Q. Huang, Y. Zhang, L. Fu, M. Wu and Y. Wu, *Journal of Materials Chemistry A*, 2020, **8**, 9313-9321.
18. M. Narayanasamy, L. Hu, B. Kirubasankar, Z. Liu, S. Angaiah and C. Yan, *Journal of Alloys and Compounds*, 2021, **882**, 160704.
19. J. Xie, G. Liu, X. Jiang, Z. Sui and S. Gao, *Ceramics International*, 2023, **49**, 10165-10171.
20. Y. Bai, H. Zhang, B. Xiang, X. Liang, J. Hao, C. Zhu and L. Yan, *ACS Appl Mater Interfaces*, 2021, **13**, 23230-23238.
21. Z. Wu, C. Lu, Y. Wang, L. Zhang, L. Jiang, W. Tian, C. Cai, Q. Gu, Z. Sun and L. Hu, *Small*, 2020, **16**, 2000698.